

Determination of Sb Isotope Ratios in Stibnite Using fs-LA-MC-ICP-MS and Two Potential Reference Materials Study

Wei Wang,^{a,b,c} Chao Li,^{a,c,*} Bo Zu,^b Jihao Zhang,^{a,c} Pengyue Yu,^{a,c,d} Hongyu Ren,^{a,c,e} Xinwei Li,^{a,c} Limin Zhou,^{a,c} and Wenjun Qu^{a,c}

^a National Research Center for Geoanalysis, Beijing 100037, P. R. China

^b School of Earth Resources, China University of Geosciences, Wuhan, 430074, P. R. China

^c Key Laboratory of Re-Os Isotope Geochemistry, China Geological Survey, Beijing 100037, P. R. China

^d State Key Laboratory of Geological Processes and Mineral Resources, School of Earth Sciences and Resources, China University of Geosciences, Beijing 100083, P. R. China

Received: January 24, 2023; Revised: February 25, 2024; Accepted: February 25, 2024; Available online: February 25, 2024.

DOI: 10.46770/AS.2024.013

ABSTRACT: This study demonstrates an analytical method for the high spatial resolution (20 μm) and high-precision determination of antimony (Sb) isotope composition in stibnite, using femtosecond laser ablation multi-collector inductively coupled plasma mass spectrometry (fs-LA-MC-ICP-MS). The potential matrix effect-inducing elements in Sb isotope composition measurements exhibit extremely low concentrations in two newly introduced natural stibnite reference materials, DC and BJS, rendering their impact virtually negligible during fs-LA-MC-ICP-MS analysis. Through reciprocal correction of DC and BJS, consistent results were achieved, aligning with those obtained by SN-MC-ICP-MS, indicating an absence of discernible matrix effects between the two samples. A comprehensive assessment was conducted to evaluate the contribution of the Sn standard solution to enhance the external precision of measurements. The 2SD of $\delta^{123}\text{Sb}$ mean values increased by 0.02‰ to 0.04‰. Adjusting the laser ablation spot size (5 μm –80 μm) to control signal intensity, we investigated the deviation in $\delta^{123}\text{Sb}$ caused by mismatched signal intensities between the sample and the reference material. The matching range of signal intensity between the reference sample and the test sample was within -40% to 140%, ensuring satisfactory precision. Additionally, once the signal intensity of ^{121}Sb exceeded 15V, the internal precision of the $^{123}\text{Sb}/^{121}\text{Sb}$ ratio no longer exhibited a significant decline. Measurements of DC and BJS were conducted using fs-LA-MC-ICP-MS, coupled with SN-MC-ICP-MS, backscattered electron maps (BSE) and elemental compositions, confirming the accuracy of this method and the homogeneity of the two potential reference materials.

INTRODUCTION

Antimony (Sb), a pivotal strategic metal, has a variety of industrial applications, including batteries, chemicals, ceramics and glass, particularly in flame retardants.¹ The primary source of Sb is Stibnite, a representative hydrothermal deposit, constituting the most economically important ore alongside other sulfide minerals.² The sustainable supply of Sb hinges upon a thorough comprehension of ore fluid evolution and the precipitation

mechanisms of stibnite within hydrothermal antimony deposits.³ Achieving these objectives requires a nuanced exploration of Sb isotopes.

Antimony (Sb) has only two stable isotopes, namely ^{121}Sb and ^{123}Sb , with relative abundances of 57.362% and 42.638%, respectively.⁴ The overall isotopic variation of Sb isotopes in various biological and geological samples in nature is approximately 2%.⁵ Isotopic fractionation of Sb is prevalent in a range of earth science processes, including redox reactions,^{6,7}

methylation in biological processes,⁸ adsorption processes,⁹⁻¹⁴ evaporation and precipitation processes,^{10, 15} mixing processes,¹⁶ and Rayleigh fractionation processes.¹⁷ This characteristic makes Sb isotope composition a valuable tracer in the field of ore deposits.^{7,15,17,18} Recent research has revealed significant variations in Sb isotope ratios in Sb-bearing mineral deposits, with a maximum $\delta^{123}\text{Sb}$ range exceeding 1%.^{6,7,15,17,19,20} As the geological database and fractionation theories of Sb isotopes continue to advance, the application prospects of Sb isotopes are poised to be extensive, offering valuable insights into redox changes in hydrothermal ore-forming systems. Moreover, Sb isotopes play a crucial role in tracing metal sources, monitoring fluid evolution, studying ore-forming processes, and guiding mineral exploration.

Over the past two decades, the Sb isotope composition has been precisely measured in pure solution form using multiple collector inductively coupled plasma mass spectrometry (MC-ICP-MS), employing thiol cotton fibers (TCF) and ion exchange chromatography.^{6,10,12,20-25} The determination of Sb isotope composition in ore minerals has predominantly concentrated on stibnite.^{7,17,19,26} While the solution nebulization (SN)-MC-ICP-MS measurement technique can achieve an overall precision better than 0.04‰ (2SD), it requires intricate and time-consuming sample preparation, along with high Sb yields. The preparation process may introduce potential isotope fractionation, and the technique lacks the capability to discern variations in Sb isotope composition at the crystal grain/sub-grain scale. Therefore, high-precision and high-spatial-resolution micro-area in situ measurement techniques are imperative for achieving microscale Sb isotope studies of minerals.²⁷ The fs-LA-MC-ICP-MS method is used to determine the stable metal isotope composition, effectively reducing the degree of isotope fractionation and matrix effects, and achieving non-matrix matching correction.^{28,29} Simultaneously, the determination of variations in isotope composition in stibnite using fs-LA-MC-ICP-MS requires the correction of instrument-induced mass discrimination through reference materials. Therefore, the acquisition of accurate $\delta^{123}\text{Sb}$ values is paramount, necessitating the use of high-quality natural stibnite standard materials. Additionally, the refinement of analytical precision is further achieved through the elements-doping method, widely applied in stable metal isotope analyses, such as Fe, Cu, Zn, Sn, etc.³⁰⁻³² While the feasibility of this approach, combined with Sn as an internal standard for correction, has been repeatedly validated,^{10,12,18,33} a comprehensive evaluation of the extent to which it enhances precision during in situ analysis has not yet been undertaken.

An optimal natural reference material should possess an ample supply to facilitate widespread utilization within the geological community.³⁴ Currently, there is a scarcity of high-quality stibnite reference materials for in situ Sb isotope analysis. In response to this gap, we have developed two natural stibnite reference

materials, namely DC and BJS, explicitly designed for in situ determination of Sb isotope composition. Utilizing fs-LA-MC-ICP-MS, we conducted measurements of the Sb isotope composition in stibnite samples (DC and BJS) to assess their potential as reference materials for in situ Sb isotope analysis. Our research findings indicate that DC and BJS exhibit consistent chemical characteristics and uniform Sb isotope composition, rendering them suitable as reference materials for in situ Sb isotope analysis.

Compared with the research conducted by Kaufmann *et al* (2021),¹⁸ this research enhances spatial resolution to 20 μm using a high-sensitivity combination of X skimmer cone and the JET sampling cone.³⁵ Additionally, we have, for the first time, evaluated the extent to which tin mass bias correction can improve external precision in situ antimony isotope analysis. We have also conducted detailed investigations into concentration effects and internal precision issues. Moreover, we have developed two natural stibnite reference materials to alleviate the shortage of antimony isotope reference materials to some extent. We found that tin mass bias correction can improve external precision by up to 0.04‰, and identified that the mismatch in signal intensity between reference materials and samples can affect measurement results. We also elucidated the influence of signal intensity on internal precision. The long-term reproducibility of the two stibnite reference materials developed in this study was determined to be 0.06‰ and 0.07‰, respectively, exceeding that of other antimony isotope reference materials.

EXPERIMENTAL

Sample description and preparation. The samples used in this study were sourced from the DaChang tin polymetallic deposit in Guangxi and the Bijiaoshan stibnite deposit in Weishan, Yunnan, both of which are categorized as hydrothermal deposits.³⁶⁻³⁸ The DaChang tin polymetallic deposit is situated in the central region of the NW-trending (Nan)Dan-(He)Chi metallogenic belt, located at the southwestern margin of the Jiangnan paleocontinent, and in the northern part of the Kunlun-Du'an-Nandan fracture zone. The exposed rock strata in this region encompass a succession of Devonian-Triassic clastic, carbonate, and siliceous rocks, with Devonian strata serving as the primary host for mineralization. The Sn polymetallic deposits in the area exhibit a zonal distribution, forming three distinct zones—east, west, and central—centered around the Longboxgai pluton in the central part of the region. The predominant occurrence of stibnite ore is concentrated in the central zone (Longboxgai-Lamao-Chashan) within the Zn-Cu-W-Sb mineralization belt.³⁹ The metallogenic stage of stibnite ore corresponded to the late phase of the intermediate stage during the metallogenic process of the DaChang tin ore. The Bijiaoshan stibnite deposit in Yunnan's Weishan is situated in the middle section

Fig. 1 The standard samples of stibnite in this study were taken from two hand specimens. (a) stibnite from the tin polymetallic deposit in DaChang, Guangxi; (b) stibnite from the Bijiashan stibnite deposit, Yunnan; (c) stibnite immobilized in an epoxy resin holder; (d) DC BSE image; (e) BJS BSE image.

of the Lanping-Simao basin of the Sanjiang Complex orogenic belt, constituting a significant component of the Weishan Yongping Polymetallic Orogenic Belt. This deposit is primarily associated with the upper Triassic carbonatite mud shale construction of the Hei Huijiang Dorsal Plateau and adheres closely to the geological layers. The principal mineral in the mining area is stibnite, presenting in various forms such as lumps, dipping, breccia, and druse.³⁸ Sample DC comprises stibnite (20%), pyrite (20%), and sphalerite (10%) as ore minerals, accompanied by potassium feldspar (30%), plagioclase feldspar (10%), quartz (10%), and other gangue minerals. On the other hand, sample BJS is predominantly composed of stibnite (90%) and quartz (10%).

In the selection of stibnite samples DC and BJS (Fig. 1a-b), a deliberate effort was made to ensure their isolation from other minerals to mitigate potential interference. High-purity particles were carefully selected, subjected to rinsing with ultrapure water, and subsequently dried. These solid samples were then mounted onto epoxy resin circular targets with a diameter of 25 millimeters.

Following exposure through sandpaper, the surfaces underwent polishing using diamond abrasive. Prior to analysis, the samples underwent ultrasonic cleaning in ultrapure water and alcohol, concluding with drying in a fume hood. A comprehensive examination of the samples utilizing a scanning electron microscope (SEM) validated their relative homogeneity, with no evidence of encapsulation by other minerals or zoning structures.

Analytical techniques

LA-ICP-MS. For the in-situ trace element analysis of stibnite using Laser Ablation-Inductively Coupled Plasma Mass Spectrometry (LA-ICP-MS), the NWR193HE ArF high-energy excimer laser ablation system (ESLG, USA) was coupled online with the Agilent 8900 ICP-MS/MS (Agilent Technologies, USA). To minimize the impact of laser ablation pulses on data quality and ensure stability, a gas homogenization device was employed before ICP-MS, effectively mitigating fluctuation effects.⁴⁰

The stibnite samples underwent laser ablation at a frequency of

Table 1. Sb isotope composition of DC and BJS by bulk SN-MC-ICP-MS

| Sample ID | N | $\delta^{123}\text{Sb}$ (‰) | 2SD (‰) |
|--------------------------------|----|-----------------------------|---------|
| DC (Micro drilled stibnite) | 12 | 0.02 | 0.04 |
| DC (Original stibnite powder) | 10 | 0.02 | 0.04 |
| Mean | | 0.02 | 0.04 |
| DC (fs-LA-MC-ICP-MS) | 62 | 0.04 | 0.07 |
| BJS (Micro drilled stibnite) | 12 | -0.37 | 0.05 |
| BJS (Original stibnite powder) | 10 | -0.36 | 0.04 |
| Mean | | -0.37 | 0.05 |
| BJS (fs-LA-MC-ICP-MS) | 62 | -0.39 | 0.06 |

Table 2. Routine operating conditions of the MC-ICP-MS and sample introduction systems

| Instruments | Operating conditions | | | | | | |
|----------------------------|-------------------------------------|-------------------|-------------------|-------------------|-------------------|-------------------|-------------------|
| MC-ICP-MS | Neptune Plus | | | | | | |
| Cup configuration | L4 | L3 | L2 | L1 | C | H1 | H3 |
| | ^{117}Sn | ^{118}Sn | ^{119}Sn | ^{120}Sn | ^{121}Sb | ^{123}Sb | ^{125}Te |
| RF power | 1200 W | | | | | | |
| Cool gas flow rate | 16 L min ⁻¹ | | | | | | |
| Auxiliary gas flow rate | 0.80 L min ⁻¹ | | | | | | |
| Carrier gas (He) flow rate | 0.58 L min ⁻¹ | | | | | | |
| Sample cone | Jet cone (orifice diameter: 1.2 mm) | | | | | | |
| Skimmer cone | X cone (orifice diameter: 0.8 mm) | | | | | | |
| High vacuum | 1 × 10 ⁻⁷ mbar | | | | | | |
| Integration time | 0.131 s | | | | | | |
| Block number | 1 | | | | | | |
| N ₂ flow rate | 5 ml s ⁻¹ | | | | | | |
| Laser ablation | ASI J-200 | | | | | | |
| Wavelength | 343 nm | | | | | | |
| Spot size | 20 μm, line length of 20–24 μm | | | | | | |
| Repetition rate | 1–3 Hz | | | | | | |
| Energy density | 1–16 J cm ⁻² | | | | | | |

8 Hz and an energy density of 8 J cm² for a duration of 50 s resulting in ablation pits approximately 40 μm in diameter. To ensure calibration and drift correction, every set of 10 samples were accompanied by one NIST SRM 610 and two MASS-1 reference materials. Subsequent data processing was carried out using the commercial software ICPMSDataCal 10.8.⁴¹ Repeated analyses consistently demonstrated precision and accuracy exceeding 10% for the majority of the analyzed elements.

SN-MC-ICP-MS. In this study, the determination of $\delta^{123}\text{Sb}$ values for two stibnite reference materials (DC and BJS) was conducted relative to the Spex Sb (USA; lot: CL 10-49SBY) standard solution using SN-MC-ICP-MS technique. $\delta^{123}\text{Sb}$ values of standard solutions Spex relative to NIST SRM 3102a ($\delta = 0$) were $0.29 \pm 0.03\%$ (2SD, n=15).³³ Pure stibnite samples were ground into powder using a micro drill under an optical microscope. Sampling was performed at distinct locations on both DC and BJS samples, and additional samples were procured from hand specimens of DC and BJS. Prior to dissolution, all samples underwent microscopic examination to confirm mineral purity.

The acquired stibnite powder (~2mg) was precisely weighed

and deposited into clean PFA vials. Subsequently, 0.5 ml of ultrapure concentrated HCl and 1 ml of ultrapure concentrated HNO₃ were added to each vial. The vials were then sealed with PFA tape and subjected to dissolution at 110°C for 24 h, followed by evaporation at 90°C. The residues were re-dissolved at 110°C for 2 hours via 2% HNO₃ and 1% HF. After a cooling period and standing for 48 hours, the remaining solution was diluted with a 1 μg g⁻¹ NIST 3102A Sn standard solution in 2% HNO₃ and 1% HF, serving as a medium for subsequent mass spectrometric analysis. As demonstrated in previous studies, ion exchange chromatography is deemed unnecessary for stibnite samples.^{17,19,21} The Spex Sb standard solution served as an external standard for DC and BJS, facilitating the comparison between laser ablation and solution analyses. All data were normalized using the reference value $\delta^{123}\text{Sb}_{\text{Spex}} = 0.02 \pm 0.04$ (2SD, n=22) for DC. The acquired values from solution measurements are presented in Table 1.

fs-LA-MC-ICP-MS. The determination of in situ Sb isotope composition in stibnite was carried out at National Research Center for Geoanalysis, using a combination of Neptune Plus MC-ICP-MS from Thermo Fisher Scientific (Germany) and a J-200 343nm Yb: Fiber femtosecond laser from Applied Spectra Instrument (USA) employing fs-LA-MC-ICPMS technology. The mass spectrometer operated in low-resolution mode and Faraday cup configuration, including an array from L4 to H3, monitor ions such as $^{117}\text{Sn}^+$, $^{118}\text{Sn}^+$, $^{119}\text{Sn}^+$, $^{120}\text{Sn}^+$, $^{121}\text{Sb}^+$, $^{123}\text{Sb}^+$, and $^{125}\text{Te}^+$ (Table 2). A combination of high-sensitivity cones, including the X skimmer cone and the JET sampling cone,³⁵ was employed and installed in the Neptune Plus interface. Helium gas served as the carrier gas during the laser ablation process. To ensure the stability of signals during laser ablation, a quartz glass homogenizer was employed, using helium gas to transport solid particles and aerosols generated during laser ablation. These were thoroughly mixed with argon and nitrogen gases before being transported to the mass spectrometer through the sample transport pipeline. For aerosolizing, the NIST 3161A Sn standard solution was utilized with the dual-channel quartz glass nebulizer and helium gas along with a small quantity of nitrogen (5 ml min⁻¹) were blended in the homogenizer through a straightforward T-shaped connector. Simultaneously, the NIST 3161A Sn standard solution was employed to fine-tune instrument parameters, encompassing helium, argon, and nitrogen flow rates, torch position, radiofrequency power settings, and ion lens settings (Fig. S1). This approach ensured optimal sensitivity and peak shapes. Detailed instrument operating conditions and measurement parameters are summarized in Table 2.

The routine data acquisition involved a series of 200 cycles, with each cycle having an integration time of 0.131 s. The laser operated at 2% output energy in constant energy mode, resulting in an energy density of approximately 1 J cm² on the sample. Given that stibnite has a Sb content of 70%, larger Sb signal intensity

could be obtained with smaller ablation spot sizes. The Sb isotope analyses were conducted in line scan mode with the laser spot diameter of 20 μm , scan length of 20 μm , scan speed of 0.6 $\mu\text{m s}^{-1}$, and laser frequency of 1-3 Hz. The scanning speed of 0.6 $\mu\text{m s}^{-1}$ is employed to enhance spatial resolution and ensure sufficient time for laser ablation. To mitigate the risk of isotope fractionation with increasing depth/diameter ratio of ablation pits over time, especially for small ablation sizes, a low ablation frequency was adopted. Under these operational conditions, both DC and BJS exhibited a signal intensity of approximately 24 V for ^{121}Sb , with the background intensity for ^{121}Sb being <0.001 V. To minimize potential position effects in Sb isotope composition analysis, all samples in this study were positioned in close proximity to the reference materials DC and BJS.

The relative difference in isotope ratio values between samples and standard were calculated with δ notation, as shown in Equation (1) (taking $^{121}\text{Sb}/^{123}\text{Sb}$ as an example), and was expressed in parts per thousand.

$$\delta^{123}\text{Sb} = \left(\frac{(^{123}\text{Sb}/^{121}\text{Sb})_{\text{Sample}}}{(^{123}\text{Sb}/^{121}\text{Sb})_{\text{Standard}}} - 1 \right) \times 1000 \quad (1)$$

The standard-sample bracketing (SSB) method was employed to correct for instrument mass bias with NIST SRM 3161A ($^{120}\text{Sn}/^{118}\text{Sn} = 1.345539$, $^{119}\text{Sn}/^{117}\text{Sn} = 1.118421$)⁴² as an internal standard. The Sb isotope ratios were initially expressed as deviations relative to DC or BJS, and then converted into values relative to Spex Sb.

$$\delta^{123}\text{Sb}_{\text{sample/Spex}} = \delta^{123}\text{Sb}_{\text{sample/house std}} + \delta^{123}\text{Sb}_{\text{house std/Spex}} \quad (2)$$

Where $\delta^{123}\text{Sb}_{\text{sample/house std}}$ represents the δ value of sample relative to our in-house reference samples, and $\delta^{123}\text{Sb}_{\text{house/Spex}}$ is the δ value of the in-house reference samples relative to Spex as determined by SN-MC-ICP-MS.

RESULTS AND DISCUSSION

Interfering elements. The application of laser ablation for isotope measurement, lacking the ion exchange chromatography matrix purification employed in solution-based methods, introduces an increased potential for matrix interference. Consequently, it becomes imperative to systematically assess the potential interfering elements that may arise during the analysis processes.⁴³ In order to investigate the impact of interfering elements on Sb isotope measurements in stibnite, 15 determinations of trace elements were randomly conducted at selected positions using LA-ICP-MS for both DC and BJS samples. The concentrations of Sb_2S_3 , Fe, Cu, Zn, Rh, Pd, Ag, Sn, and Te are listed in Table 3. Among these elements, Te, with its isotope ^{123}Te , stands out as a

potential interferent with ^{123}Sb measurements. Furthermore, Sn during the analysis has the capacity to generate $^{121}\text{Sn-H}$ and $^{123}\text{Sn-H}$, causing interference with both ^{121}Sb and ^{123}Sb , with excessive Sn content significantly impacting mass bias correction results. Additionally, Ag during the testing process can give rise to $^{107}\text{Ag}^{14}\text{N}$, $^{107}\text{A}^{16}\text{O}$, and $^{109}\text{Ag}^{14}\text{N}$ clusters, thereby causing interference with ^{121}Sb and ^{123}Sb . To investigate the impact of Sn and Te on Sb isotope composition, experiments involving element doping were conducted by Liu *et al.* (2020) and Li *et al.* (2021).^{22,44} These experiments revealed substantial deviations, approximately 0.4‰ and 0.2‰, when Te/Sb and Sn/Sb ratios were set at 0.1 and 5, respectively.¹⁸

The content of Te in stibnite was determined by LA-ICP-MS, registering values below the detection limit of ICP-MS and considerably lower than Te/Sb ratios known to induce interference. Consequently, the mass interference of ^{123}Te on ^{123}Sb can be confidently disregarded in this context. Sn serves as the internal standard element for mass bias correction, and its impact on the results of mass correction becomes significant when the Sn content in the sample exceeds 100 $\mu\text{g g}^{-1}$.¹⁸ However, the highest Sn content observed in the tested stibnite samples is 20 $\mu\text{g g}^{-1}$, rendering it insufficient to exert a substantial influence. Simultaneously, the sum of the Sn content of sample and the internal standard solution remains significantly lower than Sn/Sb required to induce an impact. In addition, an examination of trace elements in stibnite, including Fe, Cu, Zn, Rh, Pd, and Ag, based on data collected from previous studies,⁴⁵⁻⁴⁸ reveals their concentrations in stibnite to be exceptionally low. This suggests that the occurrence of substantial matrix effects on Sb isotope measurement is virtually precluded, further enhancing the reliability of the analytical results.

Internal precision. As widely acknowledged, analytical precision is predominantly influenced by signal intensity. Fig. 2 demonstrates the correlation between signal intensity (average signal intensity derived from a single analysis) of ^{121}Sb signal values and internal precision of $\delta^{123}\text{Sb}$ (2SE) for individual Sb isotope ratio measurements. With the increase in ^{121}Sb signal intensity from 0.10V to 15V, a noteworthy improvement in the internal precision of $\delta^{123}\text{Sb}$ measurements is observed, followed by no pronounced enhancement at higher signal intensities ($>15\text{V}$). In general, when the ^{121}Sb signal intensity surpasses 15V, the internal precision of $\delta^{123}\text{Sb}$ remains below 0.06‰ (2SE).

Homogeneity of DC and BJS. The measurement results of elemental characteristics are presented in Table 3 to evaluate the chemical homogeneity of stibnite samples DC and BJS. The measurements reveal that the content of Sb_2S_3 in DC ranges from 88.53 wt% to 89.54 wt%, while in BJS, it varies between 88.96 wt% and 90.59 wt%. The concentrations of other elements, namely Fe, Cu, Zn, Rh, Pd, Ag, and Te, are found to be very low. Analysis of the distribution and composition of these elements

Table 3. Trace elements data of DC and BJS stibnite

| Samples | Sb ₂ S ₃ | Fe | Cu | Zn | Rh | Pd | Ag | Sn | Te |
|---------|--------------------------------|--------------------|--------------------|--------------------|--------------------|--------------------|--------------------|--------------------|--------------------|
| | wt. % | µg g ⁻¹ | µg g ⁻¹ | µg g ⁻¹ | µg g ⁻¹ | µg g ⁻¹ | µg g ⁻¹ | µg g ⁻¹ | µg g ⁻¹ |
| DC-1 | 89.18 | 1.69 | 236.01 | 0.27 | 0.05 | 0.02 | 11.38 | 6.85 | 0.00 |
| DC-2 | 89.02 | 1.9 | 253.35 | 0.21 | 0.06 | 0.02 | 10.1 | 10.27 | 0.00 |
| DC-3 | 88.53 | 2.0 | 280.12 | 0.10 | 0.06 | 0.03 | 11.1 | 15.31 | 0.00 |
| DC-4 | 88.49 | 2.30 | 256.31 | 0.29 | 0.06 | 0.03 | 12.32 | 12.22 | 0.00 |
| DC-5 | 88.81 | 1.63 | 220.62 | 0.63 | 0.05 | 0.02 | 6.16 | 13.93 | 0.00 |
| DC-6 | 88.76 | 8.23 | 130.10 | 1.21 | 0.04 | 0.02 | 9.98 | 9.14 | 0.00 |
| DC-7 | 89.01 | 0.89 | 114.90 | 4.53 | 0.02 | 0.01 | 6.69 | 4.12 | 0.00 |
| DC-8 | 88.86 | 1.54 | 199.96 | 0.08 | 0.04 | 0.03 | 8.05 | 6.48 | 0.00 |
| DC-9 | 89.17 | 1.77 | 140.79 | 6.89 | 0.03 | 0.02 | 10.91 | 3.97 | 0.00 |
| DC-10 | 88.63 | 5.03 | 127.30 | 11.8 | 0.12 | 0.02 | 14.75 | 19.73 | 0.00 |
| DC-11 | 89.35 | 0.77 | 283.94 | 0.14 | 0.05 | 0.02 | 12.80 | 3.43 | 0.00 |
| DC-12 | 89.54 | 4.34 | 297.33 | 0.55 | 0.06 | 0.02 | 14.58 | 11.89 | 0.00 |
| DC-13 | 89.15 | 5.34 | 293.85 | 1.20 | 0.06 | 0.02 | 16.4 | 5.03 | 0.00 |
| DC-14 | 89.74 | 2.27 | 259.40 | 1.50 | 0.06 | 0.02 | 9.41 | 9.48 | 0.00 |
| DC-15 | 89.71 | 10.85 | 294.17 | 0.36 | 0.07 | 0.02 | 10.90 | 8.35 | 0.00 |
| BJS-1 | 89.19 | 1.13 | 0.95 | 0.11 | 0.00 | 0.00 | 0.09 | 0.01 | 0.00 |
| BJS-2 | 88.96 | 7.62 | 3.10 | 0.25 | 0.00 | 0.00 | 0.08 | 0.04 | 0.00 |
| BJS-3 | 89.21 | 7.3 | 6.87 | 2.25 | 0.00 | 0.01 | 0.17 | 0.05 | 0.00 |
| BJS-4 | 89.62 | 0.00 | 0.13 | 0.07 | 0.00 | 0.01 | 0.03 | 0.07 | 0.00 |
| BJS-5 | 89.68 | 0.00 | 0.07 | 0.17 | 0.00 | 0.01 | 0.02 | 0.07 | 0.00 |
| BJS-6 | 89.76 | 2.03 | 0.30 | 0.07 | 0.00 | 0.00 | 0.07 | 0.06 | 0.00 |
| BJS-7 | 89.98 | 0.57 | 2.40 | 0.04 | 0.00 | 0.01 | 0.04 | 0.06 | 0.00 |
| BJS-8 | 90.57 | 13.84 | 3.42 | 0.21 | 0.00 | 0.01 | 0.09 | 0.03 | 0.00 |
| BJS-9 | 90.73 | 5.60 | 2.13 | 0.17 | 0.00 | 0.01 | 0.07 | 0.04 | 0.00 |
| BJS-10 | 90.64 | 0.00 | 0.10 | 0.23 | 0.00 | 0.01 | 0.04 | 0.06 | 0.00 |
| BJS-11 | 90.39 | 10.97 | 6.65 | 0.49 | 0.00 | 0.01 | 0.23 | 0.07 | 0.00 |
| BJS-12 | 90.59 | 2.62 | 0.54 | 0.00 | 0.00 | 0.00 | 0.19 | 0.05 | 0.00 |
| BJS-13 | 90.19 | 5.17 | 0.97 | 0.17 | 0.00 | 0.01 | 0.19 | 0.03 | 0.00 |
| BJS-14 | 89.88 | 20.49 | 8.44 | 0.22 | 0.00 | 0.01 | 0.54 | 0.13 | 0.00 |
| BJS-15 | 89.84 | 7.10 | 0.68 | 0.41 | 0.00 | 0.01 | 0.12 | 0.14 | 0.00 |

Fig. 2 Relationship between the signal intensity of ¹²¹Sb on the relative standard error (2 RSE) for the determination of the ¹²³Sb/¹²¹Sb ratio during in situ Sb isotope analysis. Samples are stibnite from the Istamberdy Au-Sb deposit and LongKou Sb deposit.

indicates a high degree of homogeneity in both DC and BJS. Further insights into the homogeneity are obtained through the

examination of backscattered electron (BSE) images (Fig. 1d-e), which indicate the absence of mineral zoning and discernible changes in growth characteristics within the samples.

In order to evaluate the feasibility of the proposed methodology and ensure the uniformity of antimony isotope composition in reference materials, a multi-stage measurement approach was employed for both DC and BJS (Fig. 3). Through analysis at three distinct stages, the determined range of $\delta^{123}\text{Sb}_{\text{spex}}$ values was observed to be -0.03‰ to 0.09‰ for DC and -0.32‰ to -0.47‰ for BJS. Consistent results were obtained from repeated measurements on both DC and BJS, with the measured $\delta^{123}\text{Sb}_{\text{spex}}$ values for both samples conforming to a Gaussian distribution (Fig. 4a-b). Repeatability in the analysis, achieving approximately $\sim 0.03\text{‰}$ (2SD, n=9) and $\sim 0.05\text{‰}$ (2SD, n=9) within a 1-hour measurement period, was noteworthy. Furthermore, repeatability values of $\sim 0.07\text{‰}$ (2SD, n=32) and $\sim 0.06\text{‰}$ (2SD, n=32) were observed within an 8-hour measurement period. The average $\delta^{123}\text{Sb}$ values from a total of 62 analyses conducted in three stages were determined to be DC: $0.04 \pm 0.07\text{‰}$ (2SD, n=62) (Fig. 4a) and BJS: $-0.39 \pm 0.06\text{‰}$ (2SD, n=62) (Fig. 4b). These findings were consistent with the values obtained by SN-MC-ICP-MS, which were DC: $0.02 \pm 0.04\text{‰}$ (2SD, n=22) and BJS: $-0.37 \pm 0.05\text{‰}$ (2SD, n=22). Moreover, the

Fig. 3 $\delta^{123}\text{Sb}$ values of DC and BJS measured with fs-LA-MC-ICP-MS at three different stages, with error bars representing internal precision and shaded areas indicating external precision for multiple determines (2SD). The $\delta^{123}\text{Sb}$ values are the outcomes of mutual SSB correction for DC and BJS.

Fig. 4 Frequency histograms and probability density curves of $\delta^{123}\text{Sb}$ values determined by fs-LA-MC-ICP-MS: (a) DC; (b) BJS.

methodology demonstrated long-term reproducibility with values of 0.07‰ and 0.06‰, affirming the feasibility and robustness of the analytical approach. This underscores the consistent homogeneity and long-term reproducibility of DC and BJS, establishing them as suitable reference materials for Sb isotope analysis, and currently superior to other reference materials.

Sn mass bias correction. While the application of matrix-matched reference material correction presents a convenient and expeditious method for acquiring in situ Sb isotope composition results in stibnite, the analytical precision may be susceptible to fluctuations in instrument during testing. To enhance the long-term analytical precision, Sn has been used as an internal standard for mass bias correction. Despite the rigorous validation of this approach, considering the close mass number and shared chemical properties of Sn and Sb,^{9,12,18} detailed assessment has been lacking in prior studies. This study conducted continuous analyses in two phases, lasting 1 h and 3 h, respectively, under consistent laser ablation conditions, maintaining relatively constant signal

intensities. The introducing of water vapor, incorporating NIST SRM 3161A Sn as an internal standard element, allowed for Sn internal standard mass bias correction for both DC and BJS. This correction was performed in conjunction with SSB, and the results were compared with those obtained using SSB correction alone.

During a one-hour continuous analysis of DC and BJS, nine measurements of Sb isotope composition were undertaken. Employing Sn solution as an internal standard for mass bias correction, the $\delta^{123}\text{Sb}$ values for DC ranged from 0.00‰ to 0.05‰, with an average of $0.03 \pm 0.05\%$ (2SD, n=9) (Fig. 5a). In the absence of Sn solution as internal standard mass bias correction, the $\delta^{123}\text{Sb}$ values for DC ranged from -0.03‰ to 0.07‰, with an average of $0.03 \pm 0.05\%$ (2SD, n=9) (Fig. 5b). When Sn solution was utilized for internal standard mass bias correction, the $\delta^{123}\text{Sb}$ values for BJS ranged from -0.42‰ to -0.33‰, with an average of $-0.39 \pm 0.05\%$ (2SD, n=9) (Fig. 5a). Without Sn solution as internal standard mass bias correction, the $\delta^{123}\text{Sb}$ values for BJS ranged from -0.41‰ to -0.30‰, with an average of $-0.38 \pm 0.07\%$ (2SD,

Fig. 5 $\delta^{123}\text{Sb}$ values of DC and BJS at two different stages, corrected by Sn mass bias combined with SSB correction and SSB correction only) (a) $\delta^{123}\text{Sb}$ values of DC and BJS within one hour with Sn mass bias correction combined with SSB correction.(b) $\delta^{123}\text{Sb}$ values of DC and BJS within one hour with SSB correction only.(c) $\delta^{123}\text{Sb}$ values of DC and BJS within three hours with Sn mass bias correction combined with SSB correction.(d) $\delta^{123}\text{Sb}$ values of DC and BJS within three hours with SSB correction only.

n=9) (Fig. 5b). The 2SD of $\delta^{123}\text{Sb}$ average values within one hour was improved by 0.02‰. In a continuous three-hour analysis conducted under conditions of reduced instrument stability, 21 measurements of Sb isotopes were performed on both DC and BJS. The application of Sn for mass bias correction, in comparison to solely employing SSB for correction, resulted in a 2SD external precision improvement of 0.04‰ in the average $\delta^{123}\text{Sb}$ values over the three-hour period.

The results obtained both before and after Sn internal standard calibration exhibited essential consistency, while notable reductions in data deviation were achieved, successfully bringing some significantly deviating data within an acceptable error range. Importantly, the introduction of the internal standard element Sn did not produce any matrix effect. The external precision of $\delta^{123}\text{Sb}$, as indicated by 2SD, demonstrated improvement when Sn internal standard calibration was integrated with SSB in comparison to utilizing SSB alone.

Concentration effect. Stable isotopes undergo notable matrix effects during measurement via MC-ICP-MS, where observed discrepancies in measured values, resulting from concentration mismatches between samples and standards, are often associated

Fig. 6 Signal intensity matching is crucial for Sb isotope analysis results. Using DC as a reference material to correct BJS, where the signal intensity of the reference material is fixed at 12V, and the sample signal intensity varies from 3V to 38V. The x-axis represents the percentage difference in signal intensity of the sample relative to the reference material signal. The gray area indicates the error range relative to the solution value of BJS ($-0.37 \pm 0.05\text{‰}$) $\pm 0.05\text{‰}$.

with a specific form of matrix effect induced by mass discrimination effects.⁴⁹ In this experiment, a comprehensive evaluation was conducted to investigate whether the disparity in signal intensities between samples and reference materials, during fs-LA-MC-ICP-MS measurement process, would lead to deviations in the determination of Sb isotope composition. Concurrently, optimal matching ranges during the testing procedures were identified. DC was employed as reference material for correction in BJS, with measurements conducted under consistent laser ablation energy density, frequency, and line scan ablation rate. The modulation of ¹²¹Sb signal intensity was achieved by adjusting spot sizes ranging from 5 μm to 80 μm, with the signal value of ¹²¹Sb in the reference material fixed at 12V. The variation in δ¹²³Sb values were observed as the signal intensity of the sample ranged from 3V to 38V. As shown in Fig. 6, mismatches between the signal values of the reference material and the sample resulted in certain deviations. Notably, when the signal value of sample was below approximately 70% of the reference material signal value (sample at 3V, reference material at 12V), the highest deviation of approximately 0.15‰ was observed. As the sample signal value exceeded about 140% of the reference material signal value, a noticeable deviation trend appeared, reaching a maximum of 0.10‰. However, in the range where signal intensity of the sample was lower than the reference material by 40% to higher by 140%, the observed deviation was not significant. To ensure the accuracy of analysis, it is imperative to adjust the signal intensities of the sample and reference material during the testing process, maintaining their deviation within the range of -40% to 140%.

CONCLUSION

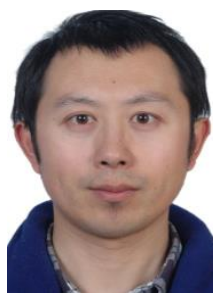
This study employed fs-LA-MC-ICP-MS technology with Sn as an internal standard correction element to establish a high spatial resolution (20 μm) and high-precision method for Sb isotope analysis in stibnite. The exceptionally low concentrations of potential interfering elements in stibnite ensure the absence of significant matrix effects on Sb isotope ratios measurement. Utilizing Sn as an internal standard for correcting isotopic fractionation, in comparison to the exclusive employment of SSB, resulted in a precision improvement of 0.02‰ and 0.04‰ in the 2SD of average δ¹²³Sb values within 1 and 3 h, respectively. Optimal measurement conditions require ensuring that the signal intensity of the sample falls within the range of -40% to 140% of the reference material. Once the signal intensity of ¹²¹Sb surpasses 15V, there is no substantial alteration in the internal precision of the ¹²³Sb/¹²¹Sb ratio. Additionally, two potential stibnite reference materials were introduced, with values determined through fs-LA-MC-ICP-MS as DC: 0.04±0.07‰ (2SD, n=62) and BJS: 0.39±0.06‰ (2SD, n=62). The values determined through SN-MC-ICP-MS were DC: 0.02±0.04‰ (2SD, n=22) and BJS:

-0.37±0.05‰ (2SD, n=22). The consistency between the values obtained by both methods, as well as the elemental composition and distribution, indicates the accuracy of this method and reliability of DC and BJS as reference materials for Sb isotope analysis.

ASSOCIATED CONTENT

Supporting information is available (Fig. S1).

AUTHOR INFORMATION



Chao Li received his BSc in 2003 from Hebei University, MSc in 2007 from Chinese Academy of Geological Sciences, and PhD in 2017 from Peking University. He is a research professor of geochemistry at National Research Center for Geoanalysis. His major research interests Re-Os isotope geochemistry and application of isotope analysis methods. He has been working as member of editorial board for *Atomic Spectroscopy*. He has published over 170 papers on technical methods and solutions to ore deposit geochronology issues.

Corresponding Author

*C. Li

Email address: Re-Os@163.com

Notes

The authors declare no competing financial interest.

ACKNOWLEDGMENTS

This study is jointly supported by the Natural Science Foundation of China (41873065) and the National Key Research and Development Program of China (2020YFA0714800). We sincerely thank Dr. Yumiao Meng from the Institute of Geochemistry, Chinese Academy of Sciences, for providing the Spex Sb reference solution. We also thank Dr. Dian Chen at the University of Chinese Academy of Sciences for enhancing the language usage in this manuscript. Additionally, we appreciate the editor and three anonymous reviewers for their insightful and detailed comments, which significantly enhanced the manuscript.

REFERENCES

1. U. Schwarz-Schampera, *Critical Metals Handbook*. 2014, 70-98. <https://doi.org/10.1002/9781118755341.ch4>

2. S. K. Haldar, *Introduction to mineralogy and petrology*. Elsevier, 2020. <https://doi.org/10.1016/b978-0-12-820585-3.00003-x>
3. H. C. Yu, K. F. Qiu, A. C. Simon, D. Wang, R. Mathur, R. Q. Wan, X. Y. Jiang, and J. Deng, *Am. Miner.*, 2023, **108**, 1213-1223. <https://doi.org/10.2138/am-2022-8490>
4. E. Anders and N. Grevesse, *Geochim. Cosmochim. Acta.*, 1989, **53**, 197-214. [https://doi.org/10.1016/0016-7037\(89\)90286-x](https://doi.org/10.1016/0016-7037(89)90286-x)
5. B. Wen, J. Zhou, A. Zhou, C. Liu, and L. Li, *Int. Biodeterior. Biodegrad.*, 2018, **128**, 109-116. <https://doi.org/10.1016/j.ibiod.2017.01.008>
6. O. Rouxel, J. Ludden, and Y. Fouquet, *Chem. Geol.*, 2003, **200**, 25-40. [https://doi.org/10.1016/s0009-2541\(03\)00121-9](https://doi.org/10.1016/s0009-2541(03)00121-9)
7. D. Wang, R. Mathur, Y. Zheng, K. Qiu, and H. Wu, *Chem. Geol.*, 2021, **584**, 347-363. <https://doi.org/10.1016/j.chemgeo.2021.120541>
8. S. Wehmeier, R. Ellam, and J. r. Feldmann, *J. Anal. At. Spectrom.*, 2003, **18**, 1001-1007. <https://doi.org/10.1039/b302242k>
9. Y. Araki, M. Tanimizu, and Y. Takahashi, *Geochim. Cosmochim. Acta.*, 2009, **73**, A49. <https://doi.org/10.1021/acs.est.3c05867.s001>
10. M. Tanimizu, Y. Araki, S. Asaoka, and Y. Takahashi, *Geochem. J.*, 2011, **45**, 27-32. <https://doi.org/10.2343/geochemj.1.0088>
11. W. Zhou, J. Zhou, X. Feng, B. Wen, A. Zhou, P. Liu, G. Sun, Z. Zhou, and X. Liu, *Environ. Sci. Technol.*, 2023, **25**, 9353-9361. <https://doi.org/10.1021/acs.est.3c01906>
12. S. Asaoka, Y. Takahashi, Y. Araki, and M. Tanimizu, *Anal. Sci.*, 2011, **27**, 25-28. <https://doi.org/10.2116/analsci.27.25>
13. W. Zhou, A. Zhou, B. Wen, P. Liu, Z. Zhu, Z. Finrock, and J. Zhou, *J Hazard Mater.*, 2022, **429**, 128317. <https://doi.org/10.1016/j.jhazmat.2022.128317>
14. B. Wen, J. Zhou, P. Tang, X. Jia, W. Zhou, and J. Huang, *J. Hazard. Mater.*, 2023, **446**, 130622. <https://doi.org/10.1016/j.jhazmat.2022.130622>
15. A. B. Kaufmann, M. Lazarov, S. Weyer, M. Števkó, S. Kiefer, and J. Majzlan, *Miner. Depos.*, 2023, **59**, 1-17. <https://doi.org/10.1007/s00126-023-01222-7>
16. E. Resongles, R. Freyrier, C. Casiot, J. Viers, J. Chmeleff, and F. Elbaz-Poulichet, *Talanta.*, 2015, **144**, 851-861. <https://doi.org/10.1016/j.talanta.2015.07.013>
17. D. Zhai, R. Mathur, S.-A. Liu, J. Liu, L. Godfrey, K. Wang, J. Xu, and J. Vervoort, *Geochim. Cosmochim. Acta.*, 2021, **306**, 84-97. <https://doi.org/10.1016/j.gca.2021.05.031>
18. A. B. Kaufmann, M. Lazarov, S. Kiefer, J. Majzlan, and S. Weyer, *J. Anal. At. Spectrom.*, 2021, **36**, 1554-1567. <https://doi.org/10.1039/d1ja00089f>
19. L. Lobo, V. Devulder, P. Degryse, and F. Vanhaecke, *J. Anal. At. Spectrom.*, 2012, **27**, 1304-1310. <https://doi.org/10.1039/c2ja30062a>
20. L. Lobo, P. Degryse, A. Shortland, and F. Vanhaecke, *J. Anal. At. Spectrom.*, 2013, **28**, 1213-1219. <https://doi.org/10.1039/c3ja50018g>
21. L. Lobo, P. Degryse, A. Shortland, K. Eremin, and F. Vanhaecke, *J. Anal. At. Spectrom.*, 2014, **29**, 58-64. <https://doi.org/10.1039/c3ja50303h>
22. J. Liu, J. Chen, T. Zhang, Y. Wang, W. Yuan, Y. Lang, C. Tu, L. Liu, and J.-L. Birck, *J. Anal. At. Spectrom.*, 2020, **35**, 1360-1367. <https://doi.org/10.1039/d0ja00136h>
23. F. Colin, R. Eléonore, F. Rémi, and C. Corinne, *J. Anal. At. Spectrom.*, 2021, **36**, 776-785. <https://doi.org/10.1039/d0ja00452a>
24. C. Ferrari, E. Resongles, R. Freyrier, and C. Casiot, *J. Anal. At. Spectrom.*, **36**, 2560-2560. <https://doi.org/10.1039/d1ja90048j>
25. G. Sun, Y. Wu, X. Feng, X. Wu, X. Li, Q. Deng, F. Wang, and X. Fu, *Chem. Geol.*, 2021, **582**, 120459. <https://doi.org/10.1016/j.chemgeo.2021.120459>
26. P. Degryse, A. J. Shortland, S. Dillis, A. van Ham-Meert, F. Vanhaecke, and P. Leeming, *J. Archaeol. Sci.*, 2020, **120**, 105195. <https://doi.org/10.1016/j.jas.2020.105195>
27. S. E. Jackson and D. Günther, *J. Anal. At. Spectrom.*, 2003, **18**, 205-212. <https://doi.org/10.1039/b209620j>
28. I. Horn and F. von Blanckenburg, *Atom. Spectrosc.*, 2007, **62**, 410-422. <https://doi.org/10.1016/j.sab.2007.03.034>
29. M. Lazarov and I. Horn, *Atom. Spectrosc.*, 2015, **111**, 64-73. <https://doi.org/10.1016/j.sab.2015.06.013>
30. R. Mathur, W. Powell, A. Mason, L. Godfrey, J. Yao, and M. E. Baker, *Geostand. Geoanal. Res.*, 2017, **41**, 701-707. <https://doi.org/10.1111/ggr.12174>
31. H. Gong, P. Guo, S. Chen, M. Duan, P. Sun, X. Wang, and Y. Niu, *Acta Geochem.*, 2020, **39**, 355-364. <https://doi.org/10.1007/s11631-019-00392-4>
32. K. Peel, D. Weiss, J. Chapman, T. Arnold, and B. Coles, *J. Anal. At. Spectrom.*, 2008, **23**, 103-110. <https://doi.org/10.1039/b710977f>
33. Y. Fang, K. Chen, Z. Bao, C. Zong, H. Yuan, and N. Lv, *Anal. Chem.*, 2022, **94**, 16746-16751. <https://doi.org/10.1021/acs.analchem.2c03420>
34. Z. Bao, N. Lv, K. Chen, Y. Luan, X. Sun, C. Zong, and H. Yuan, *Geostand. Geoanal. Res.*, 2021, **45**, 401-418. <https://doi.org/10.1111/ggr.12372>
35. S. Wu, M. Yang, Y. Yang, L. Xie, C. Huang, H. Wang, and J. Yang, *Int. J. Mass Spectrom.*, 2020, **456**, 116394. <https://doi.org/10.1016/j.ijms.2020.116394>
36. D. Wang, Y. Chen, W. Chen, H. Sang, H. Li, Y. Lu, K. Chen, and Z. Lin, *Acta Geol. Sin.-Engl. Ed.*, 2004, **78**, 132-138. <https://doi.org/10.1111/j.1755-6724.2004.tb00707.x>
37. T. Liang, D. Wang, M. Cai, Z. Chen, and H. Huang, *Acta Geol. Sin.-Engl. Ed.*, 2008, **07**, 967-977. <https://doi.org/10.1007/s11442-008-0201-7>
38. T. ZiDa, Z. Jing, and L. TengJian, *Acta Petrol. Sin.*, 2016, **32**, 2379-2391. [https://doi.org/10.1016/s0894-9166\(16\)30264-6](https://doi.org/10.1016/s0894-9166(16)30264-6)
39. M. H. Cai, J. W. Mao, T. Liang, and F. X. Wu, *Miner. Deposits.*, 2004, **02**, 225-231. https://doi.org/10.1007/3-540-27946-6_227
40. A. Tunheng and T. Hirata, *J. Anal. At. Spectrom.*, 2004, **19**, 932-934. <https://doi.org/10.1039/b402493a>
41. Y. Liu, Z. Hu, S. Gao, D. Günther, J. Xu, C. Gao, and H. Chen, *Chem. Geol.*, 2008, **257**, 34-43. <https://doi.org/10.1016/j.chemgeo.2008.08.004>
42. J. Meija, T. B. Coplen, M. Berglund, W. A. Brand, P. De Bièvre, M. Gröning, N. E. Holden, J. Irrgeher, R. D. Loss, T. Walczyk, and T. Prohaska, *Pure Appl. Chem.*, 2016, **88**, 293-306. <https://doi.org/10.1515/pac-2015-0503>
43. W. Zhang, Z. Wang, F. Moynier, E. Inglis, S. Tian, M. Li, Y. Liu, and Z. Hu, *J. Anal. At. Spectrom.*, 2019, **34**, 1800-1809. <https://doi.org/10.1039/c9ja00192a>
44. S. Li, Y. Deng, H. Zheng, X. Liu, P. Tang, J. Zhou, and Z. Zhu, *J. Anal. At. Spectrom.*, 2021, **36**, 157-164. <https://doi.org/10.1039/d0ja00367k>

45. S. Fu, R. Hu, X. Bi, N. A. Sullivan, and J. Yan, *Appl. Geochem.*, 2020, **118**, 104637.
<https://doi.org/10.1016/j.apgeochem.2020.104637>
46. A. Zhaanbaeva, K. Peng, A. Oyebamiji, and K. Asilbekov, *Acta Geochem.*, 2021, **40**, 659-675.
<https://doi.org/10.1007/s11631-021-00474-2>
47. A. B. Radková, H. E. Jamieson, K. M. Campbell, and K. A. Hudson-Edwards, *Econ. Geol.*, 2023, **118**, 621-637.
<https://doi.org/10.5382/econgeo.4937>
48. Z. Zhou, H. Li, K. Yonezu, A. Imai, and T. Tindell, *J. Geochem. Explor.*, 2023, **247**, 107177.
<https://doi.org/10.1016/j.gexplo.2023.107177>
49. X. Zhu, A. Makishima, Y. Guo, N. Belshaw, and R. O’Nions, *Int. J. Mass Spectrom.*, 2002, **220**, 21-29.
[https://doi.org/10.1016/s1387-3806\(02\)00767-4](https://doi.org/10.1016/s1387-3806(02)00767-4)
-